Experimental Neurology 392 (2025) 115355

Contents lists available at ScienceDirect

Experimental Neurology

journal homepage: www.elsevier.com/locate/yexnr

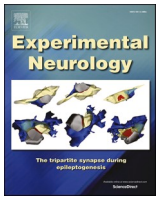

Research paper

Pathogenic role of CD169+ macrophages in neuronal loss and motor decline in NMO mice

Yuko Morita [a], Oluwaseun Fatoba [a,c], Takahide Itokazu [a,b,*], Toshihide Yamashita [a,b,c,d,*]

[a] Department of Molecular Neuroscience, Graduate School of Medicine, Osaka University, Suita, Osaka, Japan
[b] Department of Neuro-Medical Science, Graduate School of Medicine, Osaka University, Suita, Osaka, Japan
[c] WPI Immunology Frontier Research Center, Osaka, Japan
[d] Graduate School of Frontier Biosciences, Osaka University, Osaka, Japan

ARTICLE INFO

Keywords:
Neuromyelitis optica
CD169+ macrophages
Neuronal loss
Neuroinflammation
Functional deficit
Phagocytosis

ABSTRACT

Neuromyelitis optica (NMO) is a severe autoimmune inflammatory disease characterized by debilitating symptoms, such as blindness or paralysis, often following a single acute attack. However, effective acute treatments to prevent long-term sequelae are currently limited. This study aimed to investigate the role of CD169-expressing macrophages during the acute phase of NMO. We developed an NMO mouse model by injecting high-affinity AQP4-IgG with human complement into the striatum, inducing NMO-like lesions marked by astrocyte loss and infiltration of microglia/macrophages and neutrophils. Immunohistochemical analyses revealed that CD169-expressing macrophages were the predominant infiltrating cells within the lesion core. Based on this finding, we explored the therapeutic potential of blocking CD169 function to mitigate NMO. CD169+ macrophages were activated by astrocytopathy, partially through SYK signaling, leading to significant neuronal loss and motor deficits. Treatment with an anti-CD169 antibody significantly reduced neuronal loss, improved motor function, and inhibited the phagocytic activity of CD169+ macrophages. Our findings demonstrate that CD169-expressing macrophages play a critical role in exacerbating tissue damage and functional decline during the acute phase of NMO. Targeting CD169 signaling may represent a promising therapeutic strategy to reduce pathological phagocytosis and prevent secondary injury in NMO.

1. Introduction

Neuromyelitis optica (NMO) is a rare autoimmune inflammatory disorder primarily affecting the optic nerves, spinal cord, and brain (Kim et al., 2012; Nagaishi et al., 2011; Wingerchuk et al., 2006, 2007). The majority of patients with NMO are seropositive for aquaporin-4 (AQP4) antibodies, which mediate pathological effects in these regions (Lennon et al., 2004, 2005). Anti-AQP4 autoantibodies target AQP4 channels on the astrocyte foot processes, triggering astrocytopathy, loss of AQP4 expression, and local inflammation. This pathological process culminates in secondary demyelination and subsequent neuronal injury (Wu et al., 2019).

Several animal models of NMO have been developed to elucidate the molecular mechanisms of disease progression and aid in the identification of potential therapeutic targets. Monoclonal antibody therapies, including humanized anti-IL-6 and anti-CD20 antibodies, have shown efficacy in preclinical models of both multiple sclerosis (MS) and NMO and have been successfully translated into clinical application (Brod, 2020; Kim and Kim, 2020; Takeshita et al., 2021). Despite these advances, the mainstay of acute-phase intervention remains corticosteroid pulse therapy and plasma exchange, which are limited in their capacity to prevent severe sequelae (Kowarik et al., 2014). Thus, there is a pressing need for further research into the underlying pathophysiology of NMO and the development of targeted disease-specific treatments.

Recent studies have highlighted the critical role of microglia and macrophages in the pathogenesis of NMO (Asavapanumas et al., 2014;

Abbreviations: NMO, neuromyelitis optica; AQP4, Aquaporin-4; AQP4-IgG, Anti-AQP4-antibody; TMEM119, transmembrane protein 119; SYK, spleen tyrosine kinase; GFAP, glial fibrillary acidic protein; MS, multiple sclerosis; EAE, experimental autoimmune encephalomyelitis; hc, human complement; CNS, central nervous system; DARPP32, dopamine and cyclic AMP-regulated phosphoprotein-32 kDa; ICV, Intracerebroventricular; MPO, myeloperoxidase; CCL2, chemoattractants C—C motif chemokine ligand 2; ATP, adenosine triphosphate; CSF, cerebrospinal fluid.

* Corresponding authors at: Department of Molecular Neuroscience, Graduate School of Medicine, Osaka University, Suita, Osaka, Japan.
E-mail addresses: t.itokazu@molneu.med.osaka-u.ac.jp (T. Itokazu), yamashita@molneu.med.osaka-u.ac.jp (T. Yamashita).

https://doi.org/10.1016/j.expneurol.2025.115355
Received 21 March 2025; Received in revised form 15 June 2025; Accepted 21 June 2025
Available online 23 June 2025

Chen et al., 2020; Ratelade and Verkman, 2012). Generally, microglia and macrophages are key players in central nervous system (CNS) homeostasis, performing phagocytic functions that clear cellular debris and damaged cells (Yu et al., 2022). However, in response to pathological stimuli, these cells become activated, releasing neurotoxic factors, including pro-inflammatory cytokines and reactive oxygen species (ROS), thereby amplifying neuroinflammation (Li et al., 2021). Microglia/macrophage-induced inflammatory responses have been observed in NMO lesions from autopsy studies (Lucchinetti et al., 2014), and experimental depletion of these cells has been shown to mitigate NMO pathogenesis (Asavapanumas et al., 2014; Chen et al., 2020). Our previous research demonstrated that inhibiting microglia/macrophage activation with minocycline attenuates axonal degeneration and improves functional outcomes in an NMO animal model (Morita et al., 2022). Taken together, these findings suggest that targeting microglia and macrophage activation could represent a promising therapeutic approach for NMO. However, the mechanisms through which astrocytopathy influences microglia/macrophage polarization toward disease-associated phenotypes and the precise contribution of these macrophage subtypes to neurodegeneration, remain unclear.

This study aimed to investigate the role of microglia/macrophages in NMO pathology following astrocytopathy. Using a mouse model, we simulated NMO-associated tissue damage and motor deficits by administering AQP4-IgG and human complement (hc) into the striatum. Histological analyses revealed that approximately 90 % of Iba1+ cells within the lesion core were TMEM119-negative. Moreover, CD169+ macrophages were identified as the predominant macrophage subtype during the acute phase of NMO. Treatment with anti-CD169 antibodies significantly attenuated neuronal loss and motor deficits in this model. These findings indicate that CD169+ macrophages play a crucial role in the pathogenesis of NMO.

2. Materials and methods

2.1. Animals

Female wild-type C57BL/6 J mice (8–10 weeks old), sourced from Japan SLC, were used for all experiments. The animals were housed under a 12-h light/dark cycle in specific pathogen-free (SPF) conditions. All experimental protocols were reviewed and approved by the Institutional Ethics Committee of Osaka University and adhered to the Osaka University Medical School Guidelines for the Care and Use of Laboratory Animals.

2.2. NMO mouse model

An NMO mouse model was generated by intrastriatal injection of 1 μl (5 mg/ml) AQP4-IgG (E5415A) (Huang et al., 2016) or 1 μl (5 mg/ml) control IgG (Mouse IgG2A isotype control; MAB003; R&D Systems) with 0.5 μl hc (Innovative Research), as previously described (Saadoun et al., 2010), with certain modifications.

For immunohistochemistry and quantitative reverse transcriptase polymerase chain reaction (qRT-PCR), AQP4-IgG or control IgG with hc was injected unilaterally, whereas, for behavioral assessments, bilateral injections were performed.

Surgical procedures were adapted from established protocols with minor modifications (Saadoun et al., 2010). Briefly, animals were anesthetized with a mixture of butorphanol (Vetorphale®, 10 mg/kg, Meiji Seika Pharma), midazolam (Dormicum®, 8 mg/kg, Roche), and medetomidine (Domitor®, 0.6 mg/kg, Orion Pharma) and fixed in a stereotaxic apparatus (Stoelting Co.). A total volume of 1.5 μl containing AQP4-IgG and complement was slowly infused into the brain at stereotaxic coordinates: mediolateral (ML), +1.8 mm; anteroposterior (AP), +0.5 mm; and dorsoventral (DV), +3.0 mm from bregma. To reduce reflux, the glass micropipette was left in place for 5 min after injection.

2.3. Antibody treatment

Mice were randomly assigned to four experimental groups: (1) NMO mice treated with anti-CD169 antibody (0.5 mg/ml, 142402, BioLegend), (2) control mice treated with anti-CD169 antibody, (3) NMO mice treated with isotype control antibody (Rat IgG2A, 0.5 mg/ml; 400502; R&D Systems), and (4) control mice treated with isotype control antibody. A 10 μl dose of anti-CD169 or isotype control antibody was administered intracerebroventricularly (ICV) 2 days after model induction using stereotaxic coordinates: ML, +0.85 mm; AP, −0.15 mm; and DV, +2.4 mm from bregma.

2.4. Immunohistochemistry (IHC)

On days 2, 4, and 7 post-injection, mice were deeply anesthetized and perfused with 4 % paraformaldehyde (PFA) in 0.1 M phosphate buffer. The brains were harvested and post-fixed in 4 % PFA at 4 °C, followed by PBS rinsing and immersion in a 30 % sucrose solution. Brains were then embedded in Tissue-Tek O.C.T. Compound (Sakura) and stored at −80 °C. Coronal brain sections (30 μm thickness) were obtained using a cryostat (Leica Microsystems) and mounted on MAS-coated slides (Matsunami).

For IHC, sections were blocked with 3 % donkey or goat serum in PBS containing 0.1 % Triton-X (PBST) for 1 h at room temperature, followed by overnight incubation at 4 °C with primary antibodies: anti-AQP4 rabbit antibody (1:500; 59678S; Cell Signaling), anti-GFAP chicken antibody (1:1000; ab4674; Abcam), anti-Iba1 guinea pig antibody (1:500; 234–308; Synaptic Systems), anti-myeloperoxidase (MPO) rabbit antibody (1:100; PA5–16672; Thermo Fisher Scientific), anti-TMEM119 rabbit antibody (1:100; ab209064; Abcam), anti-NeuN chicken antibody (1:500; ABN91; Millipore), anti-CD206 goat antibody (1:500; AF2535; RSD), anti-CD86 rabbit antibody (1:100; ab269587; Abcam), anti-CD169 rat antibody (1:100; MCA884GA; Bio-Rad), anti-Phospho-Syk rabbit antibody (1:50; 2710S; Cell Signaling), anti-cleaved caspase-3 rabbit antibody (1:300; 9661 L; Cell Signaling), anti-DARPP32 guinea pig antibody (1:200; 382,004; Abcam), and anti-Siglec-F rat antibody (1:50; 552,125; BioLegend). Alexa Fluor secondary antibodies (1:500; Invitrogen) were applied for 1 h at room temperature, and myelin was stained with FluoroMyelin™ Green (1:300; F34651; Invitrogen) for 30 min. Nuclei were counterstained with 4′,6-diamidino-2-phenylindole, DAPI (1:1000; Dojindo).

2.5. Image analysis and IHC quantification

Images were acquired at 20 × or 40 × magnification using a SLIDEVIEW VS200 slide scanner (Evident) or FV3000 confocal microscope (Evident). Tissue damage in the NMO model, including areas of AQP4, GFAP, NeuN, and FluoroMyelin loss, was quantified using 20 × images. Double-positive TMEM119 and Iba1 cells within the lesion core (250 μm from the injection site) and periphery were quantified using 40 × images. CD169+, CD206+, and CD86+ cells were counted across the striatum at 20 × magnification. Phospho-Syk intensity and the percentage of Phospho-Syk + CD169+ cells were evaluated at 40 × magnification. Cleaved caspase-3+ cells and NeuN+ cells, as well as DARPP32 fluorescence intensity, were quantified using 20 × whole-striatum images. Three coronal sections per mouse were analyzed using ImageJ software.

2.6. Quantitative real-time PCR (qRT-PCR)

Total RNA was extracted from the striatal tissue using the RNeasy Mini Kit (QIAGEN). cDNA was synthesized using the High-Capacity cDNA Reverse Transcription Kit (Applied Biosystems), and qRT-PCR was performed on a QuantStudio 7 Flex Real-Time PCR System (Applied Biosystems). Gene expression was quantified using the following primers: GAPDH forward: 5'-TCTCCCTCACAATTTCCATCC-

3′, reverse: 5’-GGGTGCAGCGAACTTTATTG-3′, CD169 forward: 5′-GGAGATCCAGAAGCCTGTATTAG-3′, reverse: 5′- GTACAGTGGCCTTAGCATTGA-3′, CD86 forward: 5′- TGCTGATCTCAGATGCTGTTT-3′, reverse: 5′- CAGCTCACTCAGGCTTATGTT-3,’ CD206 forward: 5′- CAGCTGGACAAGGAGTTCATTA-3′, reverse: 5′- ACAACTACACAGTCAGCATCTT-3′. Relative gene expression was calculated using the $2^{-\triangle\triangle Ct}$ method, normalized to GAPDH expression.

2.7. Behavioral test

2.7.1. Grip strength test

Neuromuscular function was evaluated by measuring forelimb and hindlimb grip strength using a digital grip strength meter (Bioseb). Mice were positioned on the device, gently pulled by the tail, and the force at grip release was recorded. The average of three trials was divided by body weight to obtain normalized grip strength (N/g). Baseline readings were recorded one day prior to NMO induction, with follow-up measurements taken on days 2, 4, 7, 14, and 28 post-induction.

2.7.2. Grid walk test

Motor coordination was assessed using a grid walk test (Chao et al., 2012). Mice were placed on a metal grid (27 × 27 cm, 1.2 cm squares) and video-recorded for 2 min, during which forefoot and hindfoot placement errors were counted. Baseline testing was performed one day prior to NMO induction, with subsequent assessments on days 2, 4, 7, 14, and 28 post-induction.

2.8. Statistical analysis

All statistical analyses were performed using GraphPad Prism 10 (GraphPad Software). A two-tailed Student’s *t*-test, one-way analysis of variance (ANOVA), or two-way ANOVA with Bonferroni post-hoc corrections were applied as appropriate. Statistical significance was defined as $*p < 0.05$, $**p < 0.01$, $***p < 0.001$, and $****p < 0.0001$.

3. Results

3.1. Injection of AQP4-IgG + hc induces NMO-like lesions and motor deficits

We established an NMO mouse model by injecting 1 μl of high-affinity AQP4-IgG with 0.5 μl of complement (hc) into the striatum (Saadoun et al., 2010). We performed a histological assessment to determine whether NMO-like lesions were reproduced, as observed in a previous model(Gong et al., 2020; Saadoun et al., 2010).

To evaluate pathological changes in this model, we performed immunostaining for AQP4, FluoroMyelin, and Iba1 on days 2, 4, 7, and 28 after injection (Fig. 1A and B).

The long-term time-course analysis revealed a progressive loss of AQP4-positive areas and an increase in Iba1-positive cells from day 2, peaking at day 4, and declining by day 7. In contrast, FluoroMyelin staining revealed a gradual reduction, peaking on day 7. By day 28, AQP4 and Iba1 signals had returned to levels comparable to those of the control group, while partial FluoroMyelin loss remained (Supplemental Figs. 1B, 1D, and 1E). Based on these findings, we selected day 4 to evaluate the peak phase of AQP4 reduction (as an indicator of disease progression and immune cell infiltration) and day 7 to assess secondary tissue damage. Immunohistochemical analyses on day 4 confirmed peak pathological changes, including extensive loss of AQP4 and GFAP, increased microgliosis, and infiltration of peripheral immune cells around the antibody injection site (Figs. 1C-F). A similar tendency was observed in GFAP staining (Supplemental Fig. 1C). Notably, MPO immunoreactivity peaked earlier (on day 2) and subsequently declined, in contrast to the other markers, which exhibited maximal expression on day 4. This transient early-phase response is consistent with acute neutrophilic inflammation and is detailed in Supplemental Fig. 1F. Additionally, Siglec-F-positive eosinophils were detected in the lesion core (Supplemental Fig. 4). NeuN and FluoroMyelin staining indicated significant neuronal loss and demyelination by day 7 post-injection (Figs. 1G and1H). By day 28, both myelin and neurons had markedly recovered compared with the peak phase (Supplemental Figs. 1D and 1G).

Behavioral tests demonstrated a significant decline in motor performance following partial injection of AQP4-IgG/hc into the striatum, as evidenced by both grip strength and grid walk tests (Fig. 1I and J). Both motor function tests revealed acute impairment on day 2, and grid walk tests revealed a gradual decline up to day 7, followed by progressive recovery toward day 14; however, complete functional recovery was not observed in this period. In conjunction with the histological results in the late phase, these results suggest that although inflammatory responses were resolved by day 28, tissue repair, particularly the process of remyelination, remained incomplete. The histological changes were consistent with the observed trend of behavioral improvement. These findings suggest that astrocyte damage in the NMO model contributes to microglia/macrophage activation, neutrophil infiltration, neuronal damage, and subsequent motor impairment.

3.2. TMEM119-negative, Iba1-positive cells dominate the core of the lesion

To examine the population of microglia and macrophages, we performed double immunostaining for Iba1 and TMEM119 on day 4 post-NMO induction. No significant differences were found in the percentages of TMEM119 + Iba1+ cells between control and NMO mice in peripheral regions. However, within the lesion core, there was a drastic reduction in TMEM119 + Iba1+ cells in NMO mice, with only about 10 % of Iba1-positive cells being TMEM119+ (Figs. 2A-D).

We also performed staining for CD169, which is predominantly expressed by macrophages and is generally absent in microglia. This revealed that Iba1+, TMEM119-, CD169+ cells densely accumulated in the lesion core (Supplemental Fig. 2). TMEM119 and CD169 exhibited minimal colocalization but appeared to be in contact (Supplemental Fig. 2). This indicates that the majority of Iba1+ cells in the lesion core are likely macrophages rather than resident microglia.

3.3. CD169+ macrophages predominate in NMO lesions

We analyzed macrophage subtype distribution in the lesion core using immunohistochemistry for CD86 (M1-like macrophage marker), CD206 (M2-like macrophage marker), and CD169 (phagocytic macrophage marker)(Bogie et al., 2018; Chávez-Galán et al., 2015; Krausgruber et al., 2011; Orecchioni et al., 2019) on days 2, 4, and 7 post-NMO induction (Fig. 3A).

CD86+ macrophages were primarily located at the needle insertion site on days 2 and 4 (Fig. 3B and D). In contrast, CD206+ macrophages were detected within the lesion core (Fig. 3B and D), while CD169+ macrophages accumulated at the lesion margins, displaying a large, rounded morphology by day 4 (Fig. 3D). Quantitative analysis revealed a significant enrichment of CD169+ macrophages within the lesion core in AQP4-IgG/hc-injected mice compared to IgG isotype control/hc-injected mice across all time points (days 2, 4, and 7) (Figs. 3B-G). Similarly, CD86+ and CD206+ macrophages were significantly elevated in AQP4-IgG/hc-injected mice at day 2 but declined from days 4 to 7 (Figs. 3D-G). qRT-PCR corroborated these immunohistological findings, showing significantly higher mRNA expression levels of CD169 and CD86 on days 2 and 4 in AQP4-IgG/hc mice compared to controls at both days 2 and 4 (Supplemental Fig. 3A and 3B). CD206 mRNA expression was also significantly increased at day 2 (Supplemental Fig. 3A).

We also analyzed the phenotype of CD169+ macrophages. The number of CD169 + CD206+ cells was not significantly altered by disease induction (Fig. 3E). In the control/hc-injected group, most CD169+

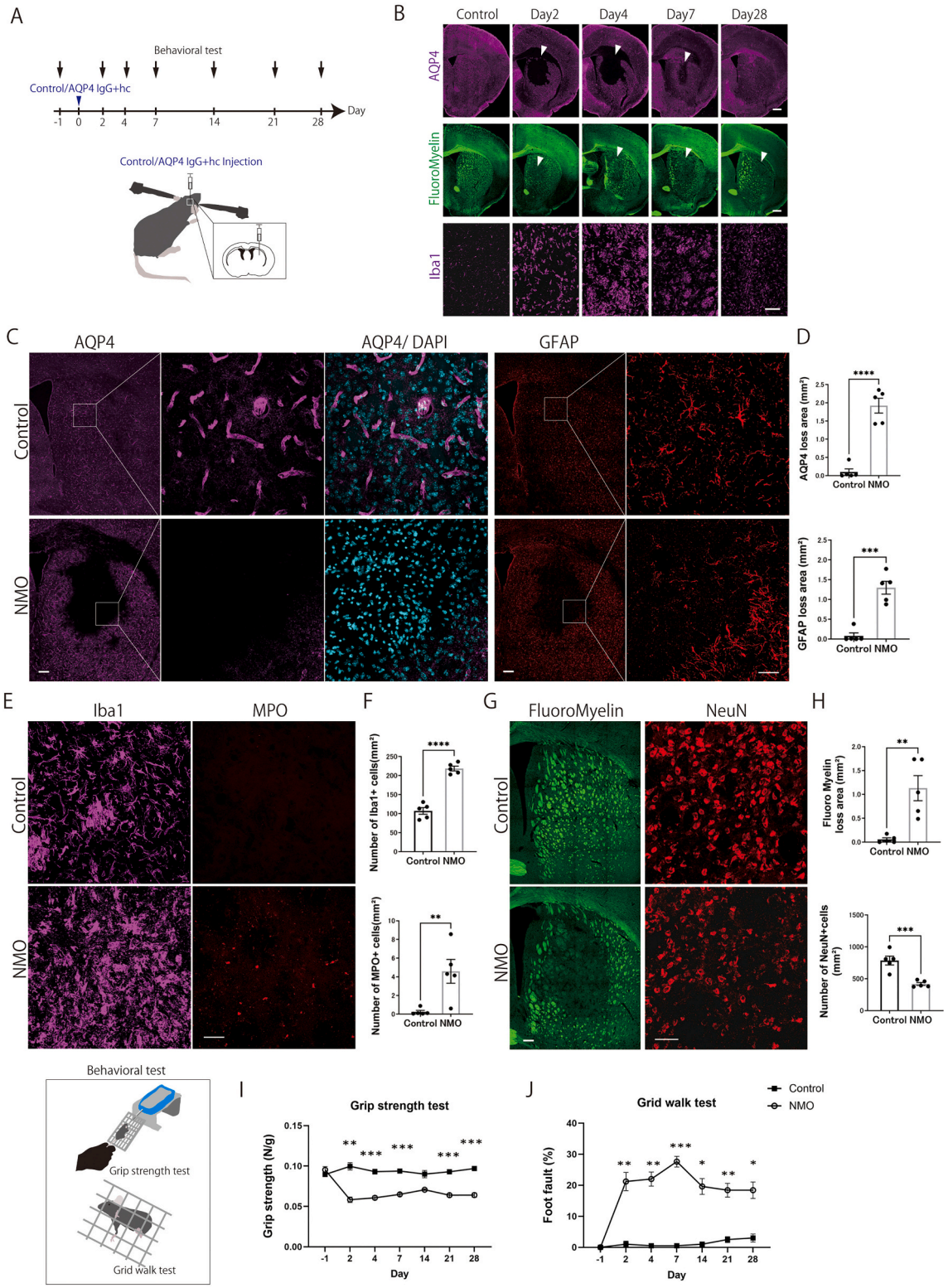

Fig. 1. Injection of AQP4-IgG + human complement induces NMO-like pathology and motor deficits. (A) Experimental timeline and procedures. Control-IgG + human complement (hc) or AQP4-IgG (E5415A) + hc was injected into the striatum. (B) Representative images showing time course data of AQP4 (magenta), FluoroMyelin (green), and Iba1 (magenta). White arrows mark the regions of loss. Scale bars: 500 μm. (C) Representative images showing AQP4 (magenta), Co-immunostaining with DAPI (blue), and GFAP (red) on day 4. Scale bars: 200 μm (Low magnification) and 50 μm (High magnification). (D) Quantification of AQP4 and GFAP loss area (mm^2) ($n = 5$). Data are shown as means ± SEM. ***$p < 0.001$, ****$p < 0.0001$, Student's *t*-test. (E) Representative images of Iba1 (magenta) and MPO (red) on day 4. Scale bars: 50 μm. (F) Quantification of Iba1+ and MPO+ cells (mm^2) (n = 5). Data are shown as means ± SEM. **$p < 0.01$, ****$p < 0.0001$, Student's *t*-test. (G) Representative images of Fluoromyelin (green) and NeuN (red) on day 7. Scale bars: 200 μm (Fluoromyelin) and 50 μm (NeuN). (H) Quantification of Fluoromyelin loss area (mm^2) and NeuN+ cells (n = 5). Data are shown as means ± SEM. **p < 0.01, ***p < 0.001, Student's *t*-test. (I, J) Quantification of grip strength and grid walk tests (n = 5). Data are shown as means ± SEM. *$p < 0.05$, **p < 0.01, ***p < 0.001, two-way ANOVA followed by Bonferroni test. (For interpretation of the references to colour in this figure legend, the reader is referred to the web version of this article.)

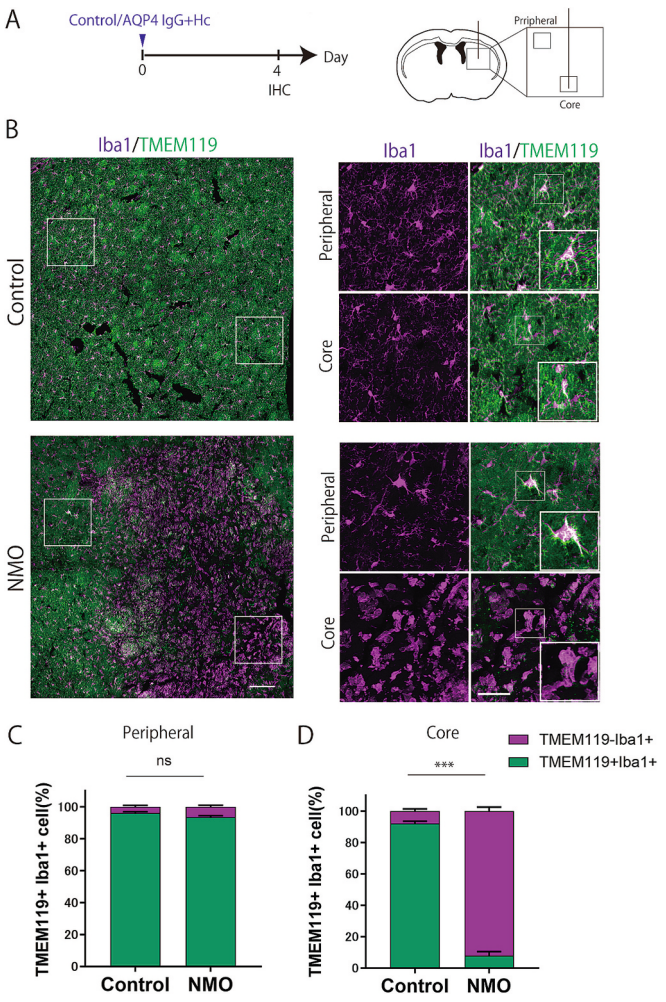

Fig. 2. TMEM119-negative Iba1-positive cells dominate the lesion core in NMO mice. (A) Experimental timeline. (B) Representative images of Iba1 (magenta) and TMEM119 (green) on day 4. Scale bars: 100 μm (Low magnification) and 50 μm (High magnification). (C, D) Quantification of the percentage of TMEM119+ Iba1+ cells (mm^2) (n = 5). Data are shown as means ± SEM. ***p < 0.001, Student's *t*-test. (For interpretation of the references to colour in this figure legend, the reader is referred to the web version of this article.)

cells colocalized with CD206+ cells, but this proportion decreased to approximately 20 % in the AQP4-IgG/hc-injected group (Fig. 3E). CD86+ cells colocalized with CD169+ cells at a high frequency in the AQP4-IgG/hc-injected group; however, such colocalization occurred in only 5 % of the total CD169+ population (Fig. 3E). Collectively, these findings confirm the presence of CD86+, CD206+, and CD169+ macrophages within the lesion core, with CD169+ macrophages representing the predominant subtype in NMO lesions.

3.4. Anti-CD169 antibody attenuates neuronal loss and motor dysfunction in AQP4-IgG-injected mice

Given the marked infiltration of CD169+ macrophages in AQP4-IgG/hc-induced lesions, we hypothesized that these macrophages contribute to neuronal damage and motor deficits. First, we checked the immunoreactivity of p-SYK, which is known to influence phagocytic activity and downstream signal of CD169 (Fig. 4A). AQP4-IgG-injected mice exhibited significantly elevated p-SYK levels compared to IgG isotype controls (Figs. 4B-D). To evaluate the effect of anti-CD169 antibody treatment, mice received an ICV injection of the antibody on day 2 post-NMO induction, and p-SYK immunostaining was performed 24 h later (Fig. 4E). Notably, anti-CD169 antibody-treated mice showed a statistically significant reduction in both p-SYK staining intensity and the number of p-SYK + CD169+ macrophages compared to isotype control-treated mice (Figs. 4F-H). However, the number of CD169+ macrophages did not significantly differ between isotype control-treated and anti-CD169 antibody-treated mice (Fig. 4I).

Macrophage-mediated neuronal damage and demyelination are hallmark pathological features of autoimmune inflammatory CNS disorders, including NMO and relapsing- remitting MS (RRMS). To assess macrophage-driven neuronal damage, we performed double immunostaining for NeuN and CD169. CD169+ macrophages were found engulfing NeuN+ neurons within the lesion core of NMO mice. However, anti-CD169 antibody treatment reduced macrophage-neuron interactions, thereby enhancing neuronal survival (Fig. 4J).

We further quantified neuronal loss through immunohistochemical staining for cleaved caspase-3, NeuN, and DARPP32 at 7 days post-NMO induction (Fig. 5A). NMO mice exhibited a significant increase in cleaved caspase-3 + NeuN+ cells relative to isotype controls (Figs. 5B-C). Treatment with the anti-CD169 antibody significantly reduced the proportion of these apoptotic neurons (Fig. 5E).

Similarly, a reduction in the total number of NeuN+ neurons and the fluorescence intensity of DARPP32+ medium spiny neurons was observed in NMO mice compared to controls, reflecting extensive neurodegeneration (Fig. 5D and F). Anti-CD169 antibody treatment significantly ameliorated neuronal loss in these mice (Fig. 5D and F).

To assess motor function, we conducted grip strength and grid-walking tests. CD169 blockade significantly improved motor deficits in NMO mice, as evidenced by enhanced grip strength and better motor coordination compared to isotype control-treated mice (Fig. 5G and H). Collectively, these findings demonstrate that CD169 inhibition not only mitigates neuronal loss but also improves motor outcomes in the NMO mouse model, highlighting the therapeutic potential of targeting CD169+ macrophages in NMO.

4. Discussion

In this study, we developed an AQP4-antibody-based NMO mouse model that replicates hallmark features of NMO, including astrocytopathy, microgliosis, and functional impairment. A key finding was the accumulation of CD169+ macrophages in lesion cores, where they actively phagocytosed both apoptotic and viable neurons, partly via the SYK signaling pathway. Our results suggest that CD169-mediated phagocytosis exacerbates neuronal damage and functional decline, making these macrophages critical contributors to NMO pathology. Notably, blocking CD169 with an anti-CD169 antibody reduced neuronal loss and improved motor coordination, highlighting the therapeutic potential of targeting this pathway in mitigating acute NMO symptoms.

NMO often results in severe disability, such as vision loss or paralysis, from a single attack, with significant implications for patient outcomes (Ma et al., 2020). Since these injuries are challenging to reverse, timely intervention during the acute phase is crucial. Recent studies have focused on developing animal models that closely mimic the clinical features of NMO to explore the role of immune cells in its pathogenesis. NMO lesions are typically characterized by the infiltration of macrophages, eosinophils, and neutrophils, with relatively few T cells (Lucchinetti et al., 2002; Saadoun et al., 2012). Prior studies have shown that reactive microglia and macrophages are more prevalent in NMO lesions compared to other inflammatory demyelinating diseases, suggesting a key role in disease progression(Iwamoto et al., 2022; Kurosawa et al., 2015; Lucchinetti et al., 2014; Misu et al., 2007). However, the precise mechanisms by which these cells contribute to neuronal injury remain unclear. Our study sought to examine the population of resident microglia and macrophages to clarify their distinct roles in NMO pathology.

We established a murine model that mimics NMO-like lesions in the striatum, characterized by significant AQP4 loss. This model was

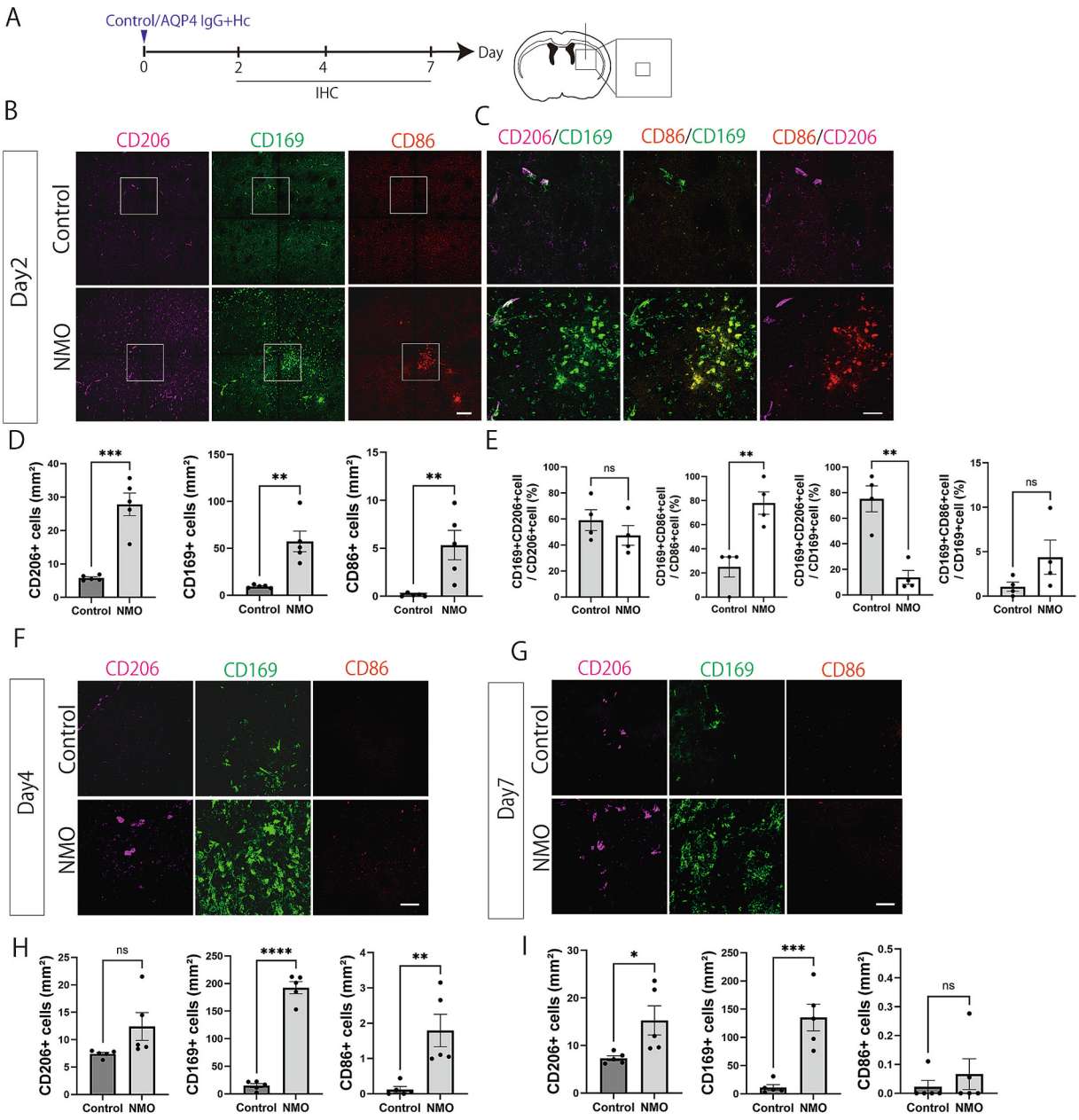

Fig. 3. CD169+ macrophages predominate around the lesion core during the acute phase of NMO. (A) Experimental timeline. Immunohistological analysis was performed on days 2, 4, and 7. (B, C) Representative images showing CD206 (magenta), CD86 (red), and CD169 (green) on day 2. Scale bars: 100 μm (Low magnification) and 50 μm (High magnification). (D, H, I) Quantification of CD206+, CD86+, and CD169+ cells on days 2, 4, and 7 (mm^2) (n = 5). Data are shown as means ± SEM. *$p < 0.05$, **p < 0.01, ***p < 0.001, ****$p < 0.0001$, Student's *t*-test. (E) Percentage of co-staining in each cell type (CD206+, CD86+, and CD169+ cells) on day 2 ($n = 4$). Data are shown as means ± SEM. **p < 0.01, Student's *t*-test. (F) Representative images of CD206 (magenta), CD86 (red), and CD169 (green) on day 4. Scale bars: 100 μm (Low magnification) and 50 μm (High magnification). (G) Representative images of CD206 (magenta), CD86 (red), and CD169 (green) on day 7. Scale bars: 100 μm (Low magnification) and 50 μm (High magnification). (For interpretation of the references to colour in this figure legend, the reader is referred to the web version of this article.)

generated using a well-established local injection approach, which enables consistent induction of NMO and facilitates pathological analysis and quantitative evaluation in mice (Asgari et al., 2013; Kim et al., 2024; Saadoun et al., 2010; Zhang and Verkman, 2013). Compared with systemic administration models, which induce widespread lesions resembling human pathology but lack regional specificity, the striatum-targeted local injection model enables the localized induction of an NMO-like lesion, thereby allowing for more detailed analysis of the pathophysiology (Huang et al., 2024), especially in terms of the temporal dynamics of inflammation, demyelination, and cell death. Regarding the location of direct injection, the optic nerve or spinal cord may be targets that result in NMO-like pathology; however, injection into such small and densely myelinated regions in mice may result in inadvertent tissue damage, and the observed pathology may actually be related to that damage (Duan and Verkman, 2020). In this regard, the striatum offers technical advantages as a target owing to well-defined anatomical landmarks and accessibility for stereotaxic surgery, allowing accurate and reproducible injections with minimal variability in location and depth. Based on these reasons, in the present study, we selected the striatum as the injection site. In addition, although NMO has traditionally been considered a disorder that primarily affects the optic nerves and spinal cord, accumulating clinical evidence has indicated the

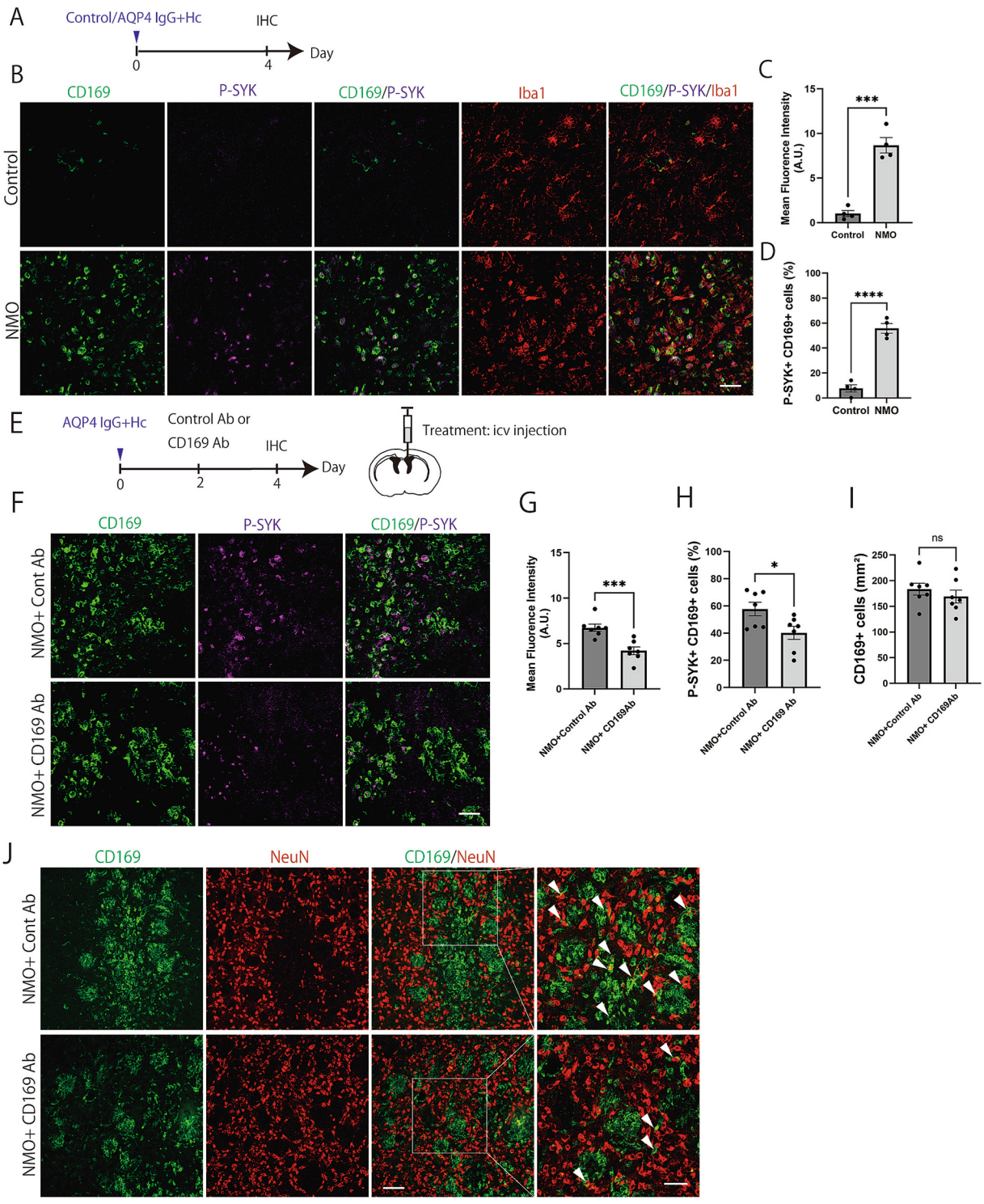

Fig. 4. Anti-CD169 antibody treatment reduces p-SYK expression and interaction between CD169+ macrophages and neurons. A) Experimental timeline. Immunohistological analysis was performed on day 4. (B) Representative images of CD169 (green), p-SYK (magenta), and Iba1 (red) on day 4. Scale bars: 50 μm. (C, D) Quantification of p-SYK fluorescence intensity and the percentage of p-SYK+ CD169+ cells on day 4 (n = 4). Data are shown as means ± SEM. ***p < 0.001, ****p < 0.0001, Student's *t*-test. (E) Experimental timeline for antibody treatment. Anti-CD169 or isotype control antibody was administered 2 days after NMO model induction via intracerebroventricular (ICV) injection. (F) Representative images of CD169 (green) and p-SYK (magenta) on day 4. Scale bars: 50 μm. (G, H) Quantification of p-SYK fluorescence intensity and the percentage of p-SYK+ CD169+ cells on day 4 (*n* = 7). (I) Quantification of CD169+ cells (mm^2) after the treatment (n = 7). Data are shown as means ± SEM. **p < 0.01, ***p < 0.001, Student's *t*-test. (J) Representative images showing CD169 (green) and NeuN (red) on day 4. White arrows indicate interactions between CD169+ cells and NeuN. Scale bars: 100 μm (Low magnification) and 50 μm (High magnification). (For interpretation of the references to colour in this figure legend, the reader is referred to the web version of this article.)

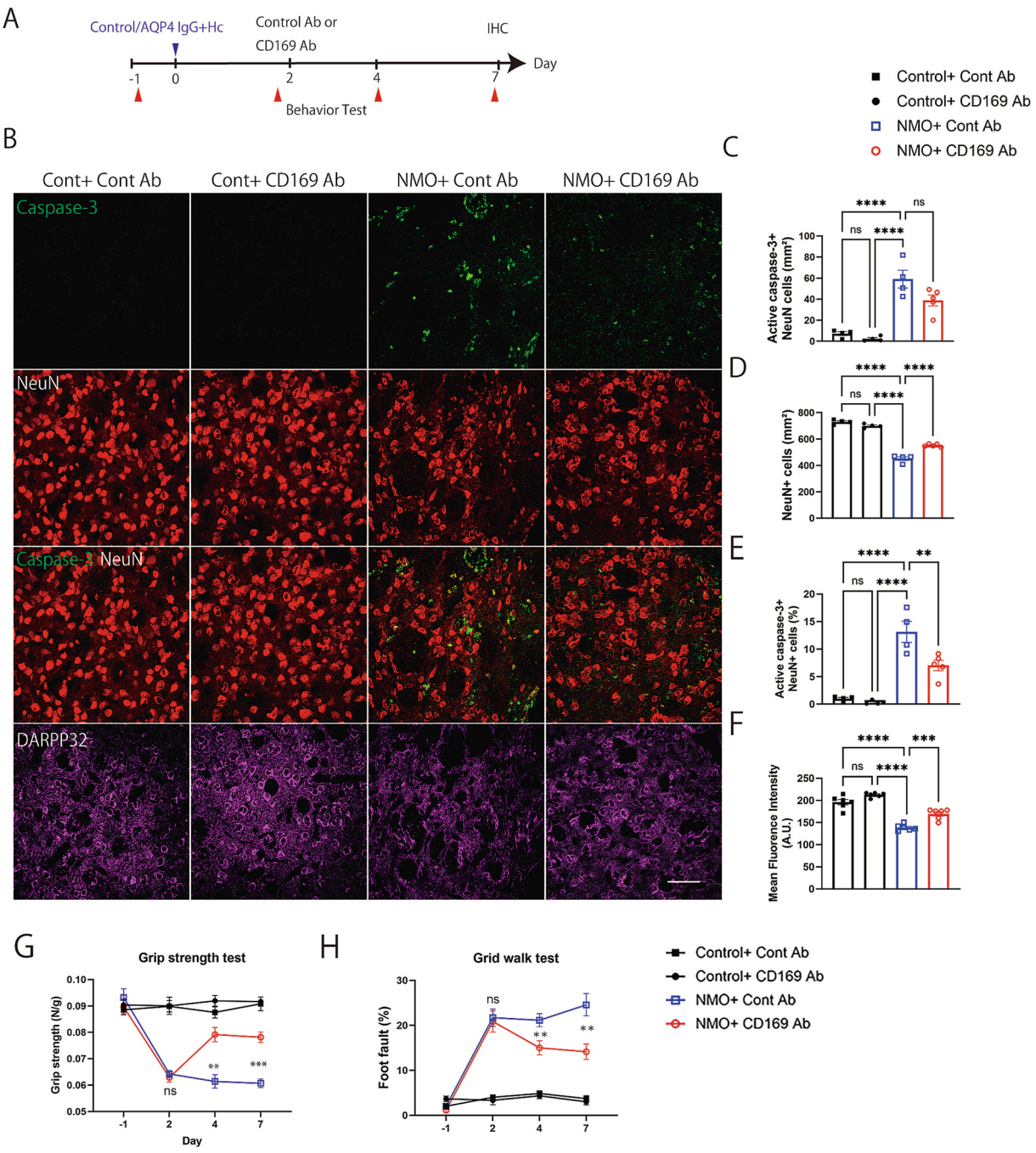

Fig. 5. Anti-CD169 antibody ameliorates neuronal loss and motor deficits in AQP4-IgG-injected mice. (A) Experimental timeline. Anti-CD169 or isotype control antibody was administered 2 days after model induction via ICV injection. Behavioral tests were conducted before NMO induction and on days 2, 4, and 7 post-induction. (B) Representative images showing cleaved caspase-3 (green), NeuN (red), and DARPP32 (magenta) on day 7. Scale bars: 50 μm. (C, D, E, F) Quantification of cleaved caspase-3+ NeuN+ cells (mm^2), number of NeuN+ cells (mm^2), percentage of cleaved caspase-3+ NeuN+ cells (mm^2), and DARPP32 fluorescence intensity on day 7 (n = 4–5). Data are shown as means ± SEM. **p < 0.01, ***p < 0.001, one-way ANOVA followed by Bonferroni test. (G, H) Quantification of grip strength and grid walk tests (n = 6–8). Data are shown as means ± SEM. **p < 0.01, ***p < 0.001, two-way ANOVA followed by Bonferroni test. (For interpretation of the references to colour in this figure legend, the reader is referred to the web version of this article.)

potential significance of other lesions to other regions including the hypothalamus, brainstem, and striatum (Kim et al., 2010, 2012; Nagaishi et al., 2011). These brain lesions are not only frequent but may also be related to disease severity and neurological symptoms, underscoring the need for experimental models that enable detailed investigation of brain-specific NMO pathology (Kim et al., 2012).

To induce the NMO pathology, we used a high-affinity anti-AQP4 antibody (E5415A), selectively binds both human and rodent AQP4 (Huang et al., 2016; Iwamoto et al., 2022; Kurosawa et al., 2015). We used human complement in combination with the anti-AQP4 antibody because the classical complement pathway in mice exhibits lower cytotoxicity than that in humans and rats (Ratelade and Verkman, 2014). The pathogenesis of NMO involves complement activation produced by the binding of anti-AQP4 antibody to AQP4 water channels on astrocytes, which leads to a marked inflammatory response (Asavapanumas et al., 2021). Additionally, mouse serum contains an inhibitor of the human classical complement pathway(Ratelade and Verkman, 2014). Thus, injection of a mixture of AQP4-IgG and human

complement is necessary to produce the major pathological features found in human NMO, including the loss of AQP4 (Asgari et al., 2013; Kim et al., 2024; Ratelade and Verkman, 2014; Saadoun et al., 2010; Zhang and Verkman, 2013). Histological analyses revealed reductions in AQP4, GFAP, FluoroMyelin, and NeuN, along with increased infiltration of Iba1+ microglia/macrophages and sporadic MPO+ neutrophils in AQP4-IgG/hc-injected mice. These pathological features closely resembled those observed in patients with NMO (Misu et al., 2007; Roemer et al., 2007). Additionally, functional impairments were confirmed via grip strength and grid walk tests.

Next, to examine the population of microglia and macrophages in our NMO model, we used TMEM119, a microglia-specific surface marker (Bennett et al., 2016; Satoh et al., 2016). Our findings showed that approximately 90 % of Iba1+ cells within the lesion core lacked TMEM119 expression, indicating that these cells are likely macrophages rather than homeostatic microglia, and predominantly driving the acute-phase pathology. This observation aligns with prior studies reporting the absence of TMEM119 expression in lesion cores during the first week after injury (Kim et al., 2024). Previous research has suggested that macrophages play a role in NMO pathogenesis, contributing to astrocyte injury (Asavapanumas et al., 2014) and secondary demyelination (Kim et al., 2024). However, the involvement of specific subtypes and their role in secondary neuronal damage had not been fully elucidated.

To address this gap, we performed immunostaining for CD86, CD206, and CD169. In our study, CD86 and CD206 transiently increased two days after model creation but subsequently declined. In contrast, CD169 was the predominant macrophage subtype during the acute phase of NMO. CD169 is a type I transmembrane glycoprotein belonging to the sialic acid-binding immunoglobulin-like lectin (Siglec) family (Munday et al., 1999). While CD169 expression is typically restricted to tissue-resident macrophages in the bone marrow, spleen, and lymph nodes (Herzog et al., 2022; Liu et al., 2020), it is also present in the perivascular space, choroid plexus, and meninges, where it identifies specialized macrophage populations distinct from microglia (Perry et al., 1992). Recent studies have highlighted the diverse roles of CD169+ macrophages, including phagocytosis, antigen presentation, antiviral responses, and antitumor activity. Moreover, CD169+ macrophages have been implicated in autoimmune diseases, such as inflammatory bowel disease, MS, and rheumatoid arthritis (Bogie et al., 2018; Li et al., 2017; Liu et al., 2020; Xiong et al., 2014). Elevated CD169 expression on CD14+ monocytes has also been observed in both patients with MS and NMO (Ostendorf et al., 2021). Bogie et al. revealed that in an EAE model, CD169+ macrophages constituted approximately 50 % of Iba1+ cells in lesion cores, and their depletion alleviated disease severity (Bogie et al., 2018). However, the presence and role of CD169+ macrophages in NMO pathogenesis remain unexplored.

Among the total population of CD169+ cells, approximately 20 % co-expressed CD206, while 5 % co-expressed CD86. Perivascular macrophages, which localize around cerebral blood vessels, are known to express both CD169 and CD206 (Rajan et al., 2020). The subset of CD169+ cells may be derived from these perivascular macrophages, and the proportion of CD169 + CD206+ cells did not significantly differ between the control and disease groups. The CD169+ cells co-expressing CD86 in this study likely have an inflammatory phenotype, as previously reported (Bogie et al., 2018). These findings indicate that CD169+ cells are abundant in the lesion core in acute NMO and may have a substantial effect on disease progression in addition to its classical pro- and anti-inflammatory roles.

To elucidate their function, we investigated the downstream signaling pathway involving p-SYK, a molecule that modulates phagocytic activity in CD169 macrophages (Guo et al., 2015; Qian et al., 2022; Tohyama and Yamamura, 2009; Wu et al., 2016). Histological analysis revealed increased p-SYK levels within NMO lesions. Treatment with an anti-CD169 antibody significantly reduced both p-SYK expression and the percentage of p-SYK + CD169+ macrophages compared to controls treated with isotype IgG. Additionally, double immunostaining for NeuN and CD169 showed that CD169+ macrophages actively phagocytosed NeuN+ neurons. However, this interaction was markedly diminished following treatment with an anti-CD169 antibody, suggesting that blocking CD169 limits neuronal loss. Li et al. previously demonstrated that microglia and macrophage activation in cerebrospinal fluid correlates with disease severity in patients with NMO (Li et al., 2022). Accordingly, we investigated whether blocking CD169 could prevent neuronal loss in AQP4-IgG/hc-induced lesions. Anti-CD169-treated mice exhibited significant preservation of NeuN+ neurons and reduced DARPP32+ neuronal loss compared to IgG-treated controls. These findings suggest that CD169-mediated phagocytosis contributes to excessive neuronal loss during acute NMO. Phagocytosis by microglia and macrophages plays a critical role in neurodevelopment, homeostasis, and pathological conditions by clearing dead cells and debris from the CNS (Yu et al., 2022). However, in pathological states, this process can result in the aberrant clearance of healthy neurons, driven by dysregulated 'find-me,' 'eat-me,' or 'don't-eat-me' signals released by stressed neurons (Brown and Neher, 2014; Butler et al., 2021; Lepiarz-Raba et al., 2023). Specifically, the 'find-me' signals released by stressed or apoptotic neurons attract phagocytic cells to the site of pathology (Neher et al., 2011; Neniskyte et al., 2011; Shimizu et al., 2023). The chemoattractants C—C motif chemokine ligand 2 (CCL2) and ATP are elevated in the CSF of human patients, supporting their involvement in NMO pathology and the idea that macrophage recruitment exacerbates neuronal loss (Ishikura et al., 2021; Narikawa et al., 2004).

Consistent with this hypothesis, anti-CD169 antibody treatment preserved NeuN+ neurons and reduced DARPP32+ medium spiny neuronal loss, indicating that CD169-mediated phagocytosis plays a central role in acute neuronal injury.

To further investigate the impact of CD169 blockade on neuroinflammation, we administered an anti-CD169 antibody and assessed functional outcomes. NMO mice treated with the anti-CD169 antibody showed improved motor performance compared to IgG-treated controls. Blocking CD169 during the acute phase selectively inhibited its phagocytic activity, thereby attenuating disability accrual. However, additional studies using genetic approaches are needed to better understand the pathological implications of CD169-mediated phagocytosis by depleting CD169+ macrophages within lesion cores.

Our immunostaining analysis also revealed an accumulation of CD169+ macrophages in the lesion core and TMEM119-negative areas. However, whether CD169+ macrophages are infiltrating macrophages or microglia remains unclear. As microglia possess high plasticity, their phenotype depends on their immediate environment (Luo and Chen, 2012). Therefore, further studies in which fate-mapping and cell-profiling tools such as single-cell RNA sequencing are used may be warranted to determine the source and gene profile of the macrophages associated with the NMO lesion core.

In conclusion, our findings highlight the pathological role of CD169+ macrophages during the acute phase of NMO, demonstrating that their phagocytic activity contributes to excessive neuronal loss and motor deficits. Blocking CD169 reduced neuronal damage and improved motor outcomes in the NMO mouse model, underscoring the therapeutic potential of targeting CD169+ macrophages to mitigate secondary injury during the acute phase of NMO.

CRediT authorship contribution statement

Yuko Morita: Writing – original draft, Visualization, Validation, Methodology, Investigation, Formal analysis, Data curation, Conceptualization. **Oluwaseun Fatoba:** Writing – review & editing, Validation, Supervision. **Takahide Itokazu:** Writing – review & editing, Validation, Supervision, Investigation, Formal analysis, Data curation, Conceptualization. **Toshihide Yamashita:** Writing – review & editing, Validation, Supervision, Project administration, Funding acquisition, Conceptualization.

Ethics approval and consent to participate

All experimental animal procedures were approved by the Ethics Committee for the Care and Use of Laboratory Animals of Osaka University Graduate School of Medicine.

Funding

This work was supported by JSPS KAKENHI (grant number 21H05049 to T.Y.) and grant-in-aid for JSPS Fellows (grant number 22J22248 to Y.M.).

Declaration of competing interest

The authors declare that they have no competing interests.

Acknowledgments

Hybridomas against AQP4 (E5415A) were provided by the RIKEN BRC through the National BioResource Project of MEXT/AMED, Japan.

Appendix A. Supplementary data

Supplementary data to this article can be found online at https://doi.org/10.1016/j.expneurol.2025.115355.

Data availability

The datasets supporting the findings of this study are available from the corresponding author upon request.

References

Asavapanumas, N., Ratelade, J., Verkman, A.S., 2014. Unique neuromyelitis optica pathology produced in naïve rats by intracerebral administration of NMO-IgG. Acta Neuropathol. 127, 539–551. https://doi.org/10.1007/s00401-013-1204-8.

Asavapanumas, N., Tradtrantip, L., Verkman, A.S., 2021. Targeting the complement system in neuromyelitis optica spectrum disorder. Expert. Opin. Biol. Ther. https://doi.org/10.1080/14712598.2021.1884223.

Asgari, N., Khorooshi, R., Lillevang, S.T., Owens, T., 2013. Complement-dependent pathogenicity of brain-specific antibodies in cerebrospinal fluid. J. Neuroimmunol. 254, 76–82. https://doi.org/10.1016/j.jneuroim.2012.09.010.

Bennett, M.L., Bennett, F.C., Liddelow, S.A., Ajami, B., Zamanian, J.L., Fernhoff, N.B., Mulinyawe, S.B., Bohlen, C.J., Adil, A., Tucker, A., Weissman, I.L., Chang, E.F., Li, G., Grant, G.A., Hayden Gephart, M.G., Barres, B.A., 2016. New tools for studying microglia in the mouse and human CNS. Proc. Natl. Acad. Sci. USA 113, E1738–E1746. https://doi.org/10.1073/pnas.1525528113.

Bogie, J.F.J., Boelen, E., Louagie, E., Delputte, P., Elewaut, D., van Horssen, J., Hendriks, J.J.A., Hellings, N., 2018. CD169 is a marker for highly pathogenic phagocytes in multiple sclerosis. Mult. Scler. J. 24, 290–300. https://doi.org/10.1177/1352458517698759.

Brod, S.A., 2020. Review of approved NMO therapies based on mechanism of action, efficacy and long-term effects. Mult. Scler. Relat. Disord. https://doi.org/10.1016/j.msard.2020.102538.

Brown, G.C., Neher, J.J., 2014. Microglial phagocytosis of live neurons. Nat. Rev. Neurosci. 15, 209–216. https://doi.org/10.1038/nrn3710.

Butler, C.A., Popescu, A.S., Kitchener, E.J.A., Allendorf, D.H., Puigdellívol, M., Brown, G. C., 2021. Microglial phagocytosis of neurons in neurodegeneration, and its regulation. J. Neurochem. https://doi.org/10.1111/jnc.15327.

Chao, O.Y., Pum, M.E., Li, J.S., Huston, J.P., 2012. The grid-walking test: assessment of sensorimotor deficits after moderate or severe dopamine depletion by 6-hydroxydopamine lesions in the dorsal striatum and medial forebrain bundle. Neuroscience 202, 318–325. https://doi.org/10.1016/j.neuroscience.2011.11.016.

Chávez-Galán, L., Olleros, M.L., Vesin, D., Garcia, I., 2015. Much more than M1 and M2 macrophages, there are also CD169+ and TCR+ macrophages. Front. Immunol. https://doi.org/10.3389/fimmu.2015.00263.

Chen, T., Lennon, V.A., Liu, Y.U., Bosco, D.B., Li, Y., Yi, M.H., Zhu, J., Wei, S., Wu, L.J., 2020. Astrocyte-microglia interaction drives evolving neuromyelitis optica lesion. J. Clin. Invest. 140, 4025–4038. https://doi.org/10.1172/JCI134816.

Duan, T., Verkman, A.S., 2020. Experimental animal models of aquaporin-4-IgG-seropositive neuromyelitis optica spectrum disorders: progress and shortcomings. Brain Pathol. https://doi.org/10.1111/bpa.12793.

Gong, Y., Zhang, Y.L., Wang, Z., Song, H.H., Liu, Y.C., Lv, A.W., Tian, L.L., Zhu, W.L., Fu, Y., Ding, X.L., Cui, L.J., Yan, Y.P., 2020. Tanshinone IIA alleviates brain damage in a mouse model of neuromyelitis optica spectrum disorder by inducing neutrophil apoptosis. J. Neuroinflammation 17, 198. https://doi.org/10.1186/s12974-020-01874-6.

Guo, M., Härtlova, A., Dill, B.D., Prescott, A.R., Gierliński, M., Trost, M., 2015. High-resolution quantitative proteome analysis reveals substantial differences between phagosomes of RAW 264.7 and bone marrow derived macrophages. Proteomics 15, 3169–3174. https://doi.org/10.1002/pmic.201400431.

Herzog, S., Fragkou, P.C., Arneth, B.M., Mkhlof, S., Skevaki, C., 2022. Myeloid CD169/Siglec1: an immunoregulatory biomarker in viral disease. Front. Med. (Lausanne). https://doi.org/10.3389/fmed.2022.979373.

Huang, P., Takai, Y., Kusano-Arai, O., Ramadhanti, J., Iwanari, H., Miyauchi, T., Sakihama, T., Han, J.Y., Aoki, M., Hamakubo, T., Fujihara, K., Yasui, M., Abe, Y., 2016. The binding property of a monoclonal antibody against the extracellular domains of aquaporin-4 directs aquaporin-4 toward endocytosis. Biochem. Biophys. Rep. 7, 77–83. https://doi.org/10.1016/j.bbrep.2016.05.017.

Huang, Y., Wang, T., Wang, F., Wu, Y., Ai, J., Zhang, Y., Shao, M., Fang, L., 2024. Scientific issues with rodent models of neuromyelitis optic spectrum disorders. Front. Immunol. 15. https://doi.org/10.3389/fimmu.2024.1423107.

Ishikura, T., Kinoshita, M., Shimizu, M., Yasumizu, Y., Motooka, D., Okuzaki, D., Yamashita, K., Murata, H., Beppu, S., Koda, T., Tada, S., Shiraishi, N., Sugiyama, Y., Miyamoto, K., Kusunoki, S., Sugimoto, T., Kumanogoh, A., Okuno, T., Mochizuki, H., 2021. Anti-AQP4 autoantibodies promote ATP release from astrocytes and induce mechanical pain in rats. J. Neuroinflammation 18. https://doi.org/10.1186/s12974-021-02232-w.

Iwamoto, S., Itokazu, T., Sasaki, A., Kataoka, H., Tanaka, S., Hirata, T., Miwa, K., Suenaga, T., Takai, Y., Misu, T., Fujihara, K., Yamashita, T., 2022. RGMa Signal in Macrophages Induces Neutrophil-Related Astrocytopathy in NMO, 91, pp. 532–547. https://doi.org/10.1002/ana.26327.

Kim, W., Kim, H.J., 2020. Monoclonal antibody therapies for multiple sclerosis and neuromyelitis optica spectrum disorder. J. Clin. Neurol. (Korea). https://doi.org/10.3988/jcn.2020.16.3.355.

Kim, W., Park, Min Su, Lee, Sang Hyun, Kim, S.-H., Jung, In Ja, Takahashi, T., Misu, T., Fujihara, K., Kim, Ho Jin, 2010. Characteristic brain magnetic resonance imaging abnormalities in central nervous system aquaporin-4 autoimmunity. Mult. Scler. J. 16, 1229–1236. https://doi.org/10.1177/1352458510376640.

Kim, W., Kim, S.-H., Huh, S.-Y., Kim, H.J., 2012. Brain abnormalities in neuromyelitis optica spectrum disorder. Mult. Scler. Int. 2012, 1–10. https://doi.org/10.1155/2012/735486.

Kim, M., Kim, W.S., Cha, H., Kim, B., Kwon, Y.N., Kim, S.M., 2024. Early involvement of peripherally derived monocytes in inflammation in an NMO-like mouse model. Sci. Rep. 14. https://doi.org/10.1038/s41598-024-51759-4.

Kowarik, M.C., Soltys, J., Bennett, J.L., 2014. The treatment of neuromyelitis optica. J. Neuroophthalmol. 34, 70–82. https://doi.org/10.1097/WNO.0000000000000102.

Krausgruber, T., Blazek, K., Smallie, T., Alzabin, S., Lockstone, H., Sahgal, N., Hussell, T., Feldmann, M., Udalova, I.A., 2011. IRF5 promotes inflammatory macrophage polarization and T H1-TH17 responses. Nat. Immunol. 12, 231–238. https://doi.org/10.1038/ni.1990.

Kurosawa, K., Misu, T., Takai, Y., Sato, D.K., Takahashi, T., Abe, Y., Iwanari, H., Ogawa, R., Nakashima, I., Fujihara, K., Hamakubo, T., Yasui, M., Aoki, M., 2015. Severely exacerbated neuromyelitis optica rat model with extensive astrocytopathy by high affinity anti-aquaporin-4 monoclonal antibody. Acta Neuropathol. Commun. 3, 82. https://doi.org/10.1186/s40478-015-0259-2.

Lennon, P.V.A., Wingerchuk, D.M., Kryzer, T.J., Pittock, S.J., Lucchinetti, C.F., Fujihara, K., Nakashima, I., Weinshenker, B.G., 2004. A serum autoantibody marker of neuromyelitis optica: distinction from multiple sclerosis. Lancet 364, 2106–2112. https://doi.org/10.1016/S0140-6736(04)17551-X.

Lennon, V.A., Kryzer, T.J., Pittock, S.J., Verkman, A.S., Hinson, S.R., 2005. IgG marker of optic-spinal multiple sclerosis binds to the aquaporin-4 water channel. J. Exp. Med. 202, 473–477. https://doi.org/10.1084/jem.20050304.

Lepiarz-Raba, I., Gbadamosi, I., Florea, R., Paolicelli, R.C., Jawaid, A., 2023. Metabolic regulation of microglial phagocytosis: implications for Alzheimer's disease therapeutics. Transl. Neurodegener. https://doi.org/10.1186/s40035-023-00382-w.

Li, Q., Wang, D., Hao, S., Han, X., Xia, Y., Li, X., Chen, Y., Tanaka, M., Qiu, C.H., 2017. CD169 expressing macrophage, a key subset in mesenteric lymph nodes promotes mucosal inflammation in dextran sulfate sodium-induced colitis. Front. Immunol. 8. https://doi.org/10.3389/fimmu.2017.00669.

Li, W., Liu, J., Tan, W., Zhou, Y., 2021. The role and mechanisms of microglia in neuromyelitis optica spectrum disorders. Int. J. Med. Sci. 18, 3059–3065. https://doi.org/10.7150/IJMS.61153.

Li, J., He, Y., Wang, H., Chen, J., 2022. Microglial/macrophage activation in the cerebrospinal fluid of neuromyelitis optica spectrum disorders. Brain Behav. 12. https://doi.org/10.1002/brb3.2798.

Liu, Y., Xia, Y., Qiu, C.H., 2020. Functions of cd169 positive macrophages in human diseases (review). Biomed. Rep. 14, 1–9. https://doi.org/10.3892/br.2020.1402.

Lucchinetti, C.F., Mandler, R.N., Mcgavern, D., Bruck, W., Gleich, G., Ransohoff, R.M., Trebst, C., Weinshenker, B., Wingerchuk, D., Parisi, J.E., Lassmann, H., 2002. A role for humoral mechanisms in the pathogenesis of Devic's neuromyelitis optica HHS public access. Brain 125 (Pt 7), 1450–1461. https://doi.org/10.1093/brain/awf151.

Lucchinetti, C.F., Guo, Y., Popescu, B.F.G., Fujihara, K., Itoyama, Y., Misu, T., 2014. The pathology of an autoimmune astrocytopathy: lessons learned from neuromyelitis optica. Brain Pathol. 83–97. https://doi.org/10.1111/bpa.12099.

Luo, X.-G., Chen, S.-D., 2012. The Changing Phenotype of Microglia from Homeostasis to Disease.

Ma, X., Kermode, A.G., Hu, X., Qiu, W., 2020. NMOSD acute attack: understanding, treatment and innovative treatment prospect. J. Neuroimmunol. https://doi.org/10.1016/j.jneuroim.2020.577387.

Misu, T., Fujihara, K., Kakita, A., Konno, H., Nakamura, M., Watanabe, S., Takahashi, T., Nakashima, I., Takahashi, H., Itoyama, Y., 2007. Loss of aquaporin 4 in lesions of neuromyelitis optica: distinction from multiple sclerosis. Brain 130, 1224–1234. https://doi.org/10.1093/brain/awm047.

Morita, Y., Itokazu, T., Nakanishi, T., Hiraga, S. Ichiro, Yamashita, T., 2022. A novel aquaporin-4-associated optic neuritis rat model with severe pathological and functional manifestations. J. Neuroinflammation 19. https://doi.org/10.1186/s12974-022-02623-7.

Munday, J., Floyd, H., Crocker, P.R., 1999. Sialic acid binding receptors (siglecs) expressed by macrophages. J. Leukoc. Biol. 66 (5), 705–711. https://doi.org/10.1002/jlb.66.5.705.

Nagaishi, A., Takagi, M., Umemura, A., Tanaka, M., Kitagawa, Y., Matsui, M., Nishizawa, M., Sakimura, K., Tanaka, K., 2011. Clinical features of neuromyelitis optica in a large Japanese cohort: comparison between phenotypes. J. Neurol. Neurosurg. Psychiatry 82, 1360–1364. https://doi.org/10.1136/jnnp-2011-300403.

Narikawa, K., Misu, T., Fujihara, K., Nakashima, I., Sato, S., Itoyama, Y., 2004. CSF chemokine levels in relapsing neuromyelitis optica and multiple sclerosis. J. Neuroimmunol. 149, 182–186. https://doi.org/10.1016/j.jneuroim.2003.12.010.

Neher, J.J., Neniskyte, U., Zhao, J.-W., Bal-Price, A., Tolkovsky, A.M., Brown, G.C., 2011. Inhibition of microglial phagocytosis is sufficient to prevent inflammatory neuronal death. J. Immunol. 186, 4973–4983. https://doi.org/10.4049/jimmunol.1003600.

Neniskyte, U., Neher, J.J., Brown, G.C., 2011. Neuronal death induced by nanomolar amyloid β is mediated by primary phagocytosis of neurons by microglia. J. Biol. Chem. 286, 39904–39913. https://doi.org/10.1074/jbc.M111.267583.

Orecchioni, M., Ghosheh, Y., Pramod, A.B., Ley, K., 2019. Macrophage polarization: different gene signatures in M1(Lps+) vs. classically and M2(LPS-) vs. alternatively activated macrophages. Front. Immunol. https://doi.org/10.3389/fimmu.2019.01084.

Ostendorf, L., Dittert, P., Biesen, R., Duchow, A., Stiglbauer, V., Ruprecht, K., Bellmann-Strobl, J., Seelow, D., Stenzel, W., Niesner, R.A., Hauser, A.E., Paul, F., Radbruch, H., 2021. SIGLEC1 (CD169): a marker of active neuroinflammation in the brain but not in the blood of multiple sclerosis patients. Sci. Rep. 11. https://doi.org/10.1038/s41598-021-89786-0.

Perry, V.H., Crocker, P.R., Gordon, S., 1992. The blood-brain barrier regulates the expression of a macrophage sialic acid-binding receptor on microglia. J. Cell Sci. 101 (Pt 1), 201–207. https://doi.org/10.1242/jcs.101.1.201.

Qian, Y., Yang, T., Liang, H., Deng, M., 2022. Myeloid checkpoints for cancer immunotherapy. Chin. J. Cancer Res. 34, 460–482. https://doi.org/10.21147/j.issn.1000-9604.2022.05.07.

Rajan, W.D., Wojtas, B., Gielniewski, B., Miró-Mur, F., Pedragosa, J., Zawadzka, M., Pilanc, P., Planas, A.M., Kaminska, B., 2020. Defining molecular identity and fates of CNS-border associated macrophages after ischemic stroke in rodents and humans. Neurobiol. Dis. 137. https://doi.org/10.1016/j.nbd.2019.104722.

Ratelade, J., Verkman, A.S., 2012. Neuromyelitis optica: Aquaporin-4 based pathogenesis mechanisms and new therapies. Int. J. Biochem. Cell Biol. https://doi.org/10.1016/j.biocel.2012.06.013.

Ratelade, J., Verkman, A.S., 2014. Inhibitor(s) of the classical complement pathway in mouse serum limit the utility of mice as experimental models of neuromyelitis optica. Mol. Immunol. 62, 104–113. https://doi.org/10.1016/j.molimm.2014.06.003.

Roemer, S.F., Parisi, J.E., Lennon, V.A., Benarroch, E.E., Lassmann, H., Bruck, W., Mandler, R.N., Weinshenker, B.G., Pittock, S.J., Wingerchuk, D.M., Lucchinetti, C.F., 2007. Pattern-specific loss of aquaporin-4 immunoreactivity distinguishes neuromyelitis optica from multiple sclerosis. Brain 130, 1194–1205. https://doi.org/10.1093/brain/awl371.

Saadoun, S., Waters, P., Bell, B.A., Vincent, A., Verkman, A.S., Papadopoulos, M.C., George, S., 2010. Intra-cerebral injection of neuromyelitis optica immunoglobulin G and human complement produces neuromyelitis optica lesions in mice. Brain 133, 349–361. https://doi.org/10.1093/brain/awp309.

Saadoun, S., Waters, P., MacDonald, C., Bell, B.A., Vincent, A., 2012. Neutrophil protease inhibition reduces neuromyelitis optica–immunoglobulin G–induced damage in mouse brain. Ann. Neurol. 71, 323–333. https://doi.org/10.1002/ana.22686. Neutrophil.

Satoh, J. Ichi, Kino, Y., Asahina, N., Takitani, M., Miyoshi, J., Ishida, T., Saito, Y., 2016. TMEM119 marks a subset of microglia in the human brain. Neuropathology 36, 39–49. https://doi.org/10.1111/neup.12235.

Shimizu, T., Schutt, C.R., Izumi, Y., Tomiyasu, N., Omahdi, Z., Kano, K., Takamatsu, H., Aoki, J., Bamba, T., Kumanogoh, A., Takao, M., Yamasaki, S., 2023. Direct activation of microglia by β-glucosylceramide causes phagocytosis of neurons that exacerbates Gaucher disease. Immunity 56, 307–319.e8. https://doi.org/10.1016/j.immuni.2023.01.008.

Takeshita, Y., Fujikawa, S., Serizawa, K., Fujisawa, M., Matsuo, K., Nemoto, J., Shimizu, F., Sano, Y., Tomizawa-Shinohara, H., Miyake, S., Ransohoff, R.M., Kanda, T., 2021. New BBB model reveals that IL-6 blockade suppressed the BBB disorder, preventing onset of NMOSD. Neurol. Neuroimmunol. Neuroinflamm. 8. https://doi.org/10.1212/NXI.0000000000001076.

Tohyama, Y., Yamamura, H., 2009. Protein tyrosine kinase, Syk: a key player in phagocytic cells. J. Biochem. https://doi.org/10.1093/jb/mvp001.

Wingerchuk, D.M., Lennon, V.A., Pittock, S.J., Lucchinetti, C.F., Weinshenker, B.G., 2006. Revised diagnostic criteria for neuromyelitis optica. Neurology 66 (10), 1485–1489. https://doi.org/10.1212/01.wnl.0000216139.44259.74.

Wingerchuk, D.M., Lennon, V.A., Lucchinetti, C.F., Pittock, S.J., Weinshenker, B.G., 2007. The spectrum of neuromyelitis optica. Lancet Neurol. https://doi.org/10.1016/S1474-4422(07)70216-8.

Wu, Y., Lan, C., Ren, D., Chen, G.Y., 2016. Induction of siglec-1 by endotoxin tolerance suppresses the innate immune response by promoting TGF-β1 production. J. Biol. Chem. 291, 12370–12382. https://doi.org/10.1074/jbc.M116.721258.

Wu, Y., Zhong, L., Geng, J., 2019. Neuromyelitis optica spectrum disorder: pathogenesis, treatment, and experimental models. Mult. Scler. Relat. Disord. https://doi.org/10.1016/j.msard.2018.12.002.

Xiong, Y.S., Cheng, Y., Lin, Q.S., Wu, A.L., Yu, J., Li, C., Sun, Y., Zhong, R.Q., Wu, L.J., 2014. Increased expression of Siglec-1 on peripheral blood monocytes and its role in mononuclear cell reactivity to autoantigen in rheumatoid arthritis. Rheumatology (United Kingdom) 53, 250–259. https://doi.org/10.1093/rheumatology/ket342.

Yu, F., Wang, Y., Stetler, A.R., Leak, R.K., Hu, X., Chen, J., 2022. Phagocytic microglia and macrophages in brain injury and repair. CNS Neurosci. Ther. https://doi.org/10.1111/cns.13899.

Zhang, H., Verkman, A.S., 2013. Eosinophil pathogenicity mechanisms and therapeutics in neuromyelitis optica. J. Clin. Invest. 123, 2306–2316. https://doi.org/10.1172/JCI67554.